Compliant force-feedback actuation for accurate robot-mediated sensorimotor interaction protocols during fMRI

Fabrizio Sergi, Andrew Erwin*, Brian Cera*, Marcia K. O'Malley

Abstract— **We propose and describe two novel force-feedback actuation systems to support accurate robot-mediated wrist motor protocols during fMRI: a co-located actuation approach and a remote actuation system based on a plastic cable-conduit transmission. To decouple the load from the non-linearities of the actuators/transmission and to enable force feedback, in both systems we include physical compliance and additional position and force sensing capabilities. Through a detailed description of the actuators design, we show how the choice between co-located and non co-located actuation influences the design of a wrist exoskeleton, to be used for robot-mediated protocols during fMRI, resulting in a parallel robot design and in a serial robot design respectively.**

I. INTRODUCTION

Understanding of the neural effects of movement therapy after neurological injury such as stroke and spinal cord injury is crucial to develop more effective rehabilitation training programs [1]. In these scenarios, robot-aided rehabilitation has been successful in introducing standardization and repeatability to movement rehabilitation techniques, paving the way for the implementation of novel and neuroscience-based rehabilitation protocols. Although it is clear that some interaction modalities do not substantially contribute to recovery [2], a full identification of the exact therapy modalities that allow a given subject or subject group to recover more effectively is far from having been accomplished.

Neuroimaging techniques such as fMRI (functional Magnetic Resonance Imaging) offer promise to shed light on such aspects. Despite its low temporal resolution, fMRI is capable of deriving a full brain map of the modulation in brain activity corresponding to a given experimental condition.

However, the same standardization, reproducibility and force display accuracy recently obtained in robot-aided rehabilitation therapy or robot-aided studies on motor control are far from being reproduced during continuous fMRI scanning. This problem is mainly due to the difficulty in introducing standard robotic technologies that allow the accurate and systematic measurement and/or assistance of human movements in MR scanners. The requirement for MR compatibility imposes technological challenges. Materials most often used in conventional robotic and mechatronic systems have ferromagnetic characteristics due to the need for mechanical properties such as strength, rigidity, and machinability [3]. Most importantly, MR-compatible robots have to address the lack of suitable actuation and measurement technologies. The commonly used electromagnetic actuators are intrinsically not MR-compatible due to their principle of operation. Efforts have been recently devoted to developing structural support and electromagnetic shielding systems that enable operation of low-impedance DC motors for motor protocols during continuous fMRI [4]; however such solutions still require the transfer of forces through long (800-3000 mm) rods, with a consequent degradation of performance accuracy, especially at high frequencies. Fluidic actuation is instead intrinsically MRI compatible: hydraulic power can be transferred through long hoses, allowing the power source (pump) to be placed outside the scanning room [5]. Fluidic actuation is however affected by high friction and by the limited dependability achievable in an environment that cannot be fully structured for continuous use with a hydraulic robot. Pneumatic systems are mainly suitable for relatively low-force applications and they have limited stiffness range and force regulation bandwidth [6]. Non-conventional actuation systems such as electrorheological fluids (ERFs) have provided an alternative way for generating resistive forces inside a MR scanner [7]. Among the systems developed so far, a promising actuation approach is represented by UltraSonic Motors (USMs), featuring intrinsic magnetic immunity, bidirectionality, high torque-to-weight ratio, small size, and compact shape [8]. Unfortunately, USMs have a very high intrinsic impedance owing to their principle of operation, hence impeding the implementation of "naif interaction controls," as defined in [9]. Previous approaches to implementation of force control through USM have either not addressed the need of compensating for the high intrinsic impedance of the robot [10], or have used force measurements in admittance control schemes that do not compensate motor non-linearities [11], compromising in both cases the accuracy of force interaction.

Other issues arise from experimental conditions that limit the possibility of motor protocols during fMRI. Most of the protocols presented so far involve shoulder and/or elbow movements [12], [13], [5], and it is well known that fMRI is very sensitive to head movements and to magnetic field changes related to the movement of body parts [14]. Both factors can lead to motion artifacts inducing false-positive activity or masking real brain activation.

For functional neuroimaging studies, it is convenient to address movements of the distal joints of the upper arm, that require movement of lower amount of body mass, in a region that is farther form the region-of-interest, and will likely induce less motion artifacts. However, assistance and measurement of movements of the distal degrees of freedom such as the wrist joint are even more challenging from a

Authors are affiliated with Rice University, Mechanical Engineering Department, Houston, TX 77005, USA. Corresponding author: fabs@rice.edu.
*A. Erwin and B. Cera contributed equally to this work.

mechatronics standpoint compared to proximal joints (i.e. shoulder and elbow) movements, due to the fine and accurate force manipulation capabilities required.

In this paper, we address the presented challenge and propose two novel actuation systems that are suitable to support interaction control protocols for wrist pointing movements. Both approaches are based on the Series Elastic Actuation architecture, a concept introduced in the mid-90s at the MIT Leg Lab [15]. We describe how this actuation concept can be translated to the needs of accurate force feedback in the MR environment by using off-the-shelf or minimally customized components in two different ways. In the first approach (i.e. co-located force-feedback actuation) we co-locate the actuator with the actuated joint where interaction force/torque is measured, thereby requiring the use of a MR-compatible actuation system. In the second approach (i.e. remote force-feedback actuation) we use a mechanical transmission composed of plastic cable-conduit system to transfer mechanical power at a large distance (5 m), thereby not requiring the use of a MR-compatible actuator, but only MR-compatible transmission and force sensing. In the following, we describe the prototypes that validate the two approaches and show how the choice of an actuation system reflects on the design of a wrist robot. We conclude the paper with a comparative analysis of the two systems performance.

II. DESIGN REQUIREMENTS

We aim to design a robot that can simultaneously measure the two most distal degrees of freedom of wrist pointing movements, i.e. flexion/extension (FE) and radial/ulnar deviation (RUD), and apply desired levels of force to guide movements or to perturb them, when a subject is subject to visually-guided motor protocols during continuous fMRI. Through measurements on a 700 mm bore diameter, 3T MR Philips Insignia scanner, we calculated the distance along the scanner axis between the scanner isocenter (typically aligned with the subject's forehead) and the edge of the cylindrical scanner to be approximately 750 mm. In those conditions, during brain imaging, the wrist of a normal-sized subject laying in the conventional supine position during scanning, with the elbow moderately flexed and supported by an angled base, would be approximately situated at the edge of the scanner.

Ideally, the wrist robot should be compatible with the movements of the human wrist, whose range of motion can be as high as 115 deg for FE and 70 deg for RUD for Activities of Daily Living [16]. However, the reported specification is more a utopian requirement. In fact, current-day fMRI imposes strong limitations, deriving from both space constraints in MR scanners and by the strong need of minimizing head movements and the distortion of the magnetic field resulting from fast and high-extent movements. Under this consideration, we decide to confine our design to a circular region with radius ± 20 deg in the end-effector plane (comprising FE and RUD joint rotation) for both degrees of freedom, around the neutral position of the wrist joint. As far as actuation requirements, we can derive from biomechanical analyses of ADL [16] that torques required are modest, with a maximum of 0.35 Nm required for both FE and RU. However, in the attempt to extend the domain of applicability of the robotic device for protocols involving motor perturbations and for study with impaired subjects who might need additional guidance, we decided to set as design requirement a minimum torque of 1.5 Nm, also in accordance with torque capabilities of wrist exoskeletons used for rehabilitation [17], [18].

III. CO-LOCATED FORCE-FEEDBACK ACTUATION

One approach to creating a MR-compatible actuation system is to co-locate the actuator with the actuated joint. In this way the actuator and transmission must all be MR-compatible. Motors suitable for this application are rotational or linear piezoelectric actuators, that are based on a non-magnetic actuation principle. Linear piezo ultrasonic drives either have insufficient power output, so we build our design around the 60 W Shinsei USR60-E3N rotary ultrasonic piezoelectric motor as the actuator. The motor is sold with a built-in velocity controller allowing for precise control of its velocity and 1000 Counts Per Turn (CPT) optical encoder, although has a nonlinear velocity characteristics. In fact, using the built-in velocity controller, the minimum velocity that can be regulated is 15 rpm, and the Shinsei built-in velocity controller does not provide means to regulate motor velocity at low amplitudes.

Considering the requirement of supporting rotations around two orthogonal axes, the best manipulator structure that allows integration of the co-located actuation architecture is a parallel design, since parallel manipulators reduce the inertial/gravitational loading on proximal joints, caused by the lower mass-to-torque ratio of MR-compatible actuators. To this aim, given the opportunity of replicating the kinematic structure of the RiceWrist [17], and to conduct experiments that matched the same task performed during therapy and during fMRI, we selected the 3RPS kinematic scheme of the RiceWrist. Among other advantages of this choice, with this solution we are able to convert three degrees of freedom into the 2DOF rotations of the handle, within a range of motion that is compatible to the one needed for motor protocols in MRI (and wrist rehab therapy). To satisfy

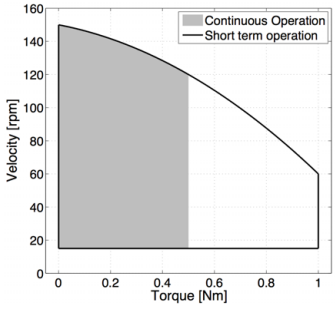

Fig. 1. Torque vs. velocity curve for the ultrasonic motor included in the co-located force feedback actuation scheme. (from manufacturer)

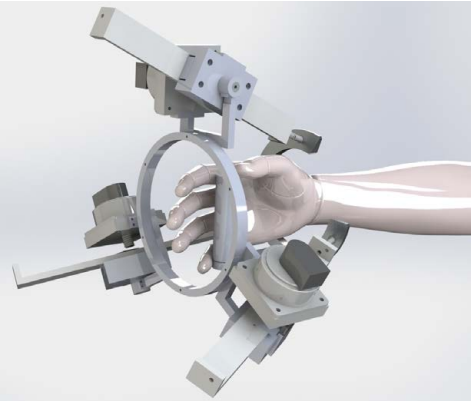

Fig. 2. Concept of the MR-compatible RiceWrist, composed of three Revolute-Prismatic-Spherical legs to connect the base frame to the moving platform, that follows wrist joint rotations when the subject grasps the handle. The series of ceramic ball bearings and brass-and-plastic universal joints approximates the spherical joints.

space requirements, the handle is reversed, thus resulting in a end-effector type design, shown in Fig. 2. Moreover, since the Shinsei motor is non-backdriveable, we include compliance and force sensing in our design, to achieve backdriveability through force-feedback control.

The 1DOF modules as seen in Fig. 3 consist of an ultrasonic motor (SHINSEI USR60-E3N), a threaded pulley (12 mm pitch radius, 2 mm pitch) connected to the motor shaft, a cable transmission (0.4 mm diameter SpiderWire Stealth Teflon-coated polyethlene cable), two custom-designed pretensioned phosphor bronze extension springs (stiffness: 1.9 N/mm, max force: 36 N, pre-tension: 12 N), a custom 3D printed ABS plastic slider and a non-magnetic linear ceramic ball bearing, produced by DelTron Precision Inc. The rotational motion of the USM is converted to linear motion through a cable transmission which connects the motor's rotations to two springs in parallel to the load, which are connected to a slider through eye bolts. The total travel of the linear actuator is 35 mm, accounting also for the reduction in workspace required by maximum springs deflection under loading.

Since the USR60 is non-backdrivable, measurement of interaction force required the use of series elasticity, and measurement of springs deflection. This is accomplished through measurement of both motor rotation (1000 CPT incremental encoder) and of the load displacement, through a 500 Lines Per Inch (LPI) linear optical encoder (US Digital), resulting in a linear quantization of 0.01 mm for load displacement (quantization of 0.04 N for measurement of interaction force). A picture of the assembled prototype is reported in Fig. 3. A complete characterization of the interaction control capabilities of this actuation architecture has been included in a recently submitted journal paper [19], demonstrating an achievable impedance range of 23 dB, with a bandwidth of 4 Hz, for low stiffness values (10% of the physical spring stiffness), and of 8 Hz for higher stiffness.

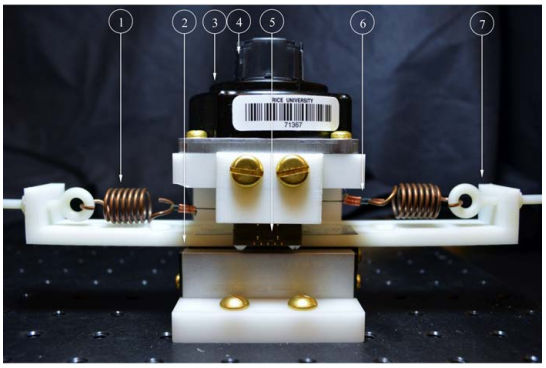

Fig. 3. Actuator of the co-located system. (1) phosphor bronze extension spring, (2) ceramic linear ball bearings, (3) Shinsei piezoceramic motor, (4) Motor-side rotary optical encoder, (5) Linear encoder, (6) cable transmission, (7) slider with plastic eyebolts.

IV. REMOTE FORCE-FEEDBACK ACTUATION

The other approach pursued in this study is based on a mechanical transmission composed of a polymeric cable-conduit system, similar to the one presented in [20] for position control applications, to transfer mechanical power outside the 5 gauss line (>3 m from the scanner edge for a 3 T scanner) thereby enabling the adoption of non-MR-compatible actuators as power source. To deal with the non-linearities and avoid reflecting the high friction of the long cable-conduit system, we implement compliant force sensing at the distal end of the transmission. To demonstrate this approach, a rotary actuator design is similarly implemented. The rotary actuator can be included in a 2 DOF system capable of supporting wrist flexion-extension and radial-ulnar deviation during continuous fMRI. Since this configuration does not result in excessive gravitational and inertial loading to the distal actuated joints (i.e. the weight and inertia of actuators is decoupled from the load by the cable-conduit transmission), we are able to pursue a simpler serial R-R design and still guarantee 2DOF wrist rotations with isotropic reflected inertia properties.

To analyze the performance achievable through this actuation approach, a 1 DOF prototype was designed and built. The prototype is comprised of both a motor-side (non MR-compatible) and load-side assembly, and consists of the following components: a standard rotary DC motor (150W Maxon RE40), a threaded aluminum spool on the motor shaft, a plastic cable-conduit transmission (composed of a 1.2 mm inner-diamater PFA conduit and of a 0.4 mm diameter SpiderWire Stealth Teflon-coated polyethlene cable, both approximately 2.5 m long), supporting clamps, a translatable motor mount that serve to pre-tension the cable-conduit system, plastic frame for support of mating elements, ceramic rotary ball bearings, plastic capstan arch, custom-designed torsion spring and machined shaft. A view of the load-side assembly is shown in Fig. 4, that includes a diagram describing the force transfer within the different components.

The exposed cable is wrapped around the threaded aluminum spool attached to the motor shaft and passes through

the external conduit clamped down on the motor-side using a stationary support. The cable-conduit system then extends to the remote load-side assembly where the outer conduit is again clamped using a stationary support. The exposed cable is then secured to the capstan using setscrews. A pretension is applied on the motor side by forcing the translatable motor mount away from the motor-side clamped cable position through the use of two bolts pressed against a face of the motor mount and threaded into the stationary cable support. By increasing this displacement until a sufficient pre-tension on the cable is achieved, cable slippage and/or unwrapping in the motor side is prevented. On the load-side, the capstan is connected to the shaft using a ball bearing, allowing for independent rotation of either component, and in series with the custom-designed torsional spring, which is rigidly attached to the shaft. Torque is transferred from the capstan arch to the outer arms of the double spiral through pegs mounted with interference; the spiral transfers the applied torque to the load shaft (mounted on the hexagonal profile cut in the inner spring annulus) through its compliance, thus embodying the series elastic actuation architecture. The shaft is supported by a frame with rotary ceramic ball bearings at either end. The DC motor is equipped with an optical incremental encoder (500 pulses per revolution) that results in 0.18 deg quantization in the measurement of motor rotation. Load-side displacement is measured using incremental rotary optical encoders, comprised of hub-disks and reading heads (2500 CPR, resulting in a rotation quantization error of 0.036 deg), at two locations: i) at the capstan, measuring the motor-side rotation of the spring, and ii) at the end of the shaft closest to the applied load, measuring the load-side spring rotation.

A Delrin torsion spring was designed for this application, based on the disk-shaped double spiral shape presented in [21]. An iterative FEM design optimization method was conducted to obtain the following requirements: *i)* Minimum Safety Factor equal to 2, when the maximum torque of 2 N m was applied; *ii)* Stiffness between 0.15 and 0.2 N m/deg (so to reduce the maximum torque measurement quantization below 10 mNm, or 0.5% of the max output torque)), *iii)*; a compact form factor so that it could be easily machined through inexpensive laser-cutting. Through SolidWorks built-in finite analysis tool, spring shape was optimized within a few design iterations, modifying the width of the spiral arms and the total spiral angle, resulting in a theoretical stiffness pedicured by FEM analysis equal to 0.175 Nm/deg, with a minimum Safety Factor of 2.5 for the loading condition described, in an element with an outer diameter of 104 mm and thickness of 6.35 mm.

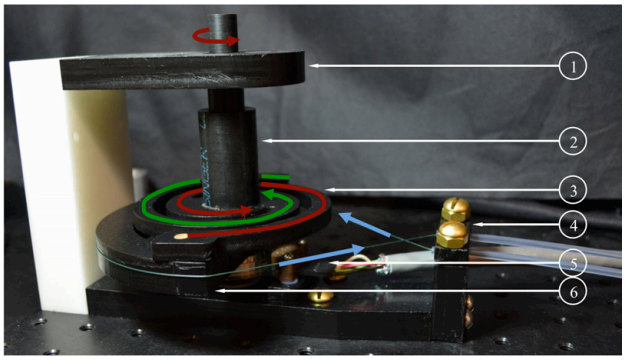

Fig. 4. Prototype of the 1 DOF rotary remote force-feedback actuation system. 1) Delrin frame; 2) Delrin output shaft; 3) Spiral torsion spring; 4) supporting clamps for the cable-conduit system; 5) Optical encoder; 6) Capstan arch. The load-side encoder is not included in the assembly. The arrows describe the configuration resulting from motion applied on the wires (as indicated by the light blue arrows), when the shaft is grounded. Red and green curved arrows indicate the pathway of force propagation from the wire, through the spiral, to the blocked shaft.

A. *Prototype characterization*

The custom torsion spring was characterized by applying forces on the capstan arch through a ATI Nano 17 force sensor, and blocking the load-side output shaft. Measuring the resulting displacement with the optical encoder mounted in the non blocked side of the spring, a load vs. displacement curve was derived, as reported in Fig. 6, for both loading and unloading conditions, in ccw and cw directions. A linear regression analysis determined a torsion spring rate of 0.177 $\mathrm{N\,m\,deg^{-1}}$, with a coefficient of determination R^2=0.994. Remarkably, the predicted and calculated spring rates differ by less than 1%. Some non-linearities are present when the derivative of the load applied changes sign, arising from both friction between the sliding surfaces of the torsion spring and capstan arch and from the inherent viscoelasticity of Delrin. Due to these non-linearities, the maximum non-linearity error throughout the $\pm$2 N m range is 0.18 N m, around 9% of the peak output characteristics.

A further set of experiments was conducted to characterize the transfer of motion between the motor side and the load side, which is affected by the non-linearities introduced by the cable-conduit system. As modeled in [22], due to the combination of compliance of the cable-conduit system and of static and viscous friction between the cable and the conduit, the force needed to overcome friction in the transmission generates a significant deformation of the cable,

Fig. 5. FEM simulation of Delrin spring, with inner annulus blocked and loading torque applied through the capstan arch. The two outer ends of the double spiral are rigidly connected through the capstan arch. The predicted stiffness equals 0.175 $\mathrm{N\,m\,deg^{-1}}$, and the resulting maximum von Mises stress is 2.5 times smaller than Delrin yield stress (62MPa).

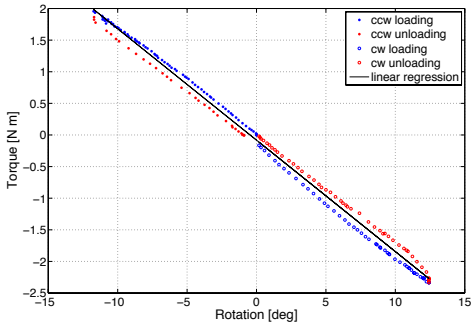

Fig. 6. Torque vs. rotation for the rotary actuator in blocked-output conditions.

before motion is fully transferred to the distal end of the cable. This results in an input-output non-linearity, that can be described as kinematic backlash. To quantify this phenomenon, the motor was commanded a sinusoidal position profile, with 0.5 Hz frequency, and 120 deg amplitude. The result of this experiment, as expressed in the input/output static position response, is shown in Fig. 7(a). Through multiple linear regression, the backlash parameters of the static model, m (slope), c_r and c_l (y-axis intercept for positive and negative motor velocity), were determined as $m = 6.6$, $c_r = 13.6$, $c_l = -22.2$. An explicit backlash compensation scheme was implemented, following the block diagram model described in Fig. 7(b), that uses the smooth backlash inverse (BI) [23]. The performance of the BI controller was assessed by commanding the load to follow a sinusoidal position profile, with amplitude 20 deg, at 0.5 Hz and 2 Hz - Fig. 7(c)-(d). The BI algorithm was compared to two linear proportional feedback control actions, one closed on the load encoder measurement (FB-L) and the other closed on the motor encoder measurement (FB-M). The FB-M controller does not compensate for the backlash, and results in a maximum error of 5 deg. Using the measurement from the load and/or proper transmission modeling, it is instead possible to compensate for the backlash, resulting in a maximum error of 0.4 deg (for the BI controller), and 0.5 deg (for the FB-L). Despite the small reduction in maximum error provided by the BI controller, compared to the FB-L, the BI algorithm minimizes the phase lag, and also guarantees avoidance of limit cycles for higher feedback gain values [24]. Finally, the implemented BI controller was used for a force-control scheme during interaction with a subject that applied perturbations to the output shaft, as schematized in Fig. 7(e). The controller is described in Fig. 7(f), and is based on the cascaded force-velocity controller previously proposed for compliant actuation [25], with the addition of the explicit non-linear compensation action, to minimize the effects of backlash. The result of a transparency experiment, obtained by setting $\tau_{des} = 0$, are shown in Fig. 7, for manually applied perturbations. It can be seen that the maximum torque error, as measured through the deflection of the torsion spring, amounts to only 0.1 Nm, demonstrating the feasibility of transparent interaction control through the remote actuation

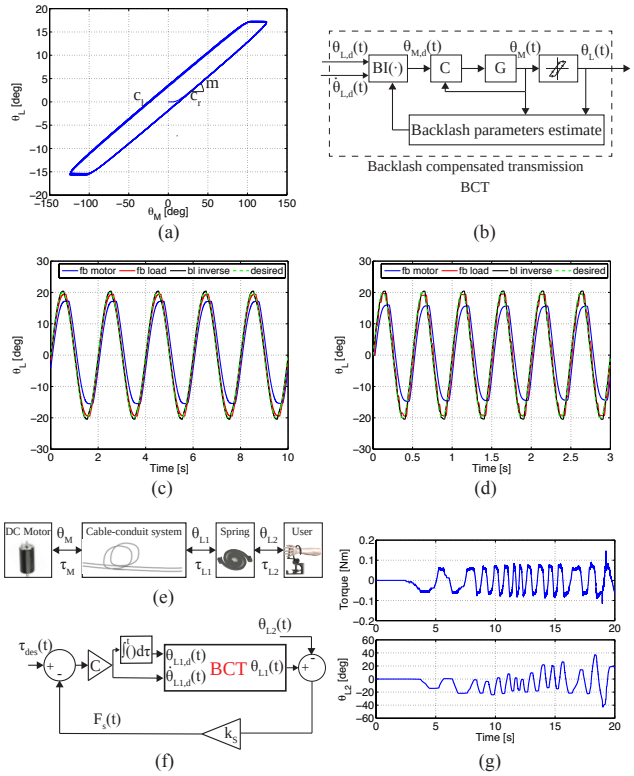

Fig. 7. Characterization and control of the remote actuation architecture. (a) Input-output nonlinearity of the transmission, as described by parameters m, c_r and c_l. (b) Block diagram of the Backlash Inverse (BI) compensation scheme implemented, as described in [22]. (c) Characterization of position control performance of the BI controller, and comparison with the FB-L and FB-M controllers, for a sinusoidal load position profile, with amplitude 20 deg and frequency 0.5 Hz and (d) 2 Hz. (e) Block diagram describing the components, labeling and set-up of the remote actuation system during the human perturbation experiment, in which the motor was controlled through the cascaded force-velocity controller, described in (f). (g) Results of the perturbation experiment, defined in terms of the interaction torque $\tau_s = k_s(\theta_{L2} - \theta_{L1})$ measured when $\tau_{des} = 0$.

architecture.

V. CONCLUSIONS

In this paper, we presented two actuation systems based on force-feedabck, designed for inclusion in an MR-compatible robot for wrist movement protocols during fMRI. The first approach explored inclusion of the actuator in the scanner, with consequent need of adoption of an MR-compatible actuator. As a consequence of the choice of co-locating the actuators in the MR-compatible robot, a parallel robotic design was chosen, since it allows to optimally distribute the loads introduced by the MR-compatible motors selected and to increase manipulator structural stiffness. The second approach pursued in this paper involved a cable, remote actuation architecture, that enable placement of actuators remotely from the scanner room and hence enables employment of non MR-compatible actuators, such as DC motors. The choice of a free-form cable-conduit, series elastic transmission enabled decoupling the motor inertial and gravitational loading from

the load side, allowing for a serial robot design.

The co-located solution resulted in a linear SE actuator, which required simple, but necessarily custom-manufactured extension spring, that were made in phosphor bronze, because simpler and more commercially available components could either not be used for MR-compatibility or would not be capable of satisfying the required specifications in terms of force measurement accuracy. Through the special linear ceramic ball bearings, customized from the manufacturer for our application to remove any aluminum components for improved MR-compatiblity, slider friction was reduced to negligible levels, (i.e. static friction lower than 0.01 N, and viscous friction lower than 0.01 $\mathrm{N\,s\,m^{-1}}$). The main disadvantage of the parallel design pursued is the need for spherical joints, that are typically not manufactured without including any ferrous metals. In our current system, we are substituting the spherical joints required for the parallel design with the series of a revolute joint and a universal joint, that can be made out of non-ferrous materials, at the cost of reducing the available workspace of the robot, to a value still within the design specification. Another disadvantage of the co-located actuation is the introduction of non-linearities in the transfer of motion and forces to the compliant element, with the potential of reducing the upper limit of control parameters resulting in coupled stability during interaction.

The non-colocated solution resulted in a serial manipulator, with simpler kinematics and reduction of actuators inertial/gravitational loading through the cable-conduit system. Also in this case, spring design required the manufacture of an ad-hoc component, but a good linear compliant element could be obtained through a relatively simple machining process, making use of inexpensive material and machining process. A drawback of the remote actuation solution is the increased design complexity, in terms of number of components needed, and the increased set-up time required for installing of the actuator in the MRI, that necessitates cables pre-tensioning.

VI. ACKNOWLEDGMENT

This work was supported in part by a TIRR Memorial Hermann Pilot Project grant, by the NSF CNS-1135916 grant, by the NSF GRFP 0940902 and by the H133P0800007-NIDRR-ARRT fellowships.

REFERENCES

[1] A. R. Carter, L. T. Connor, and A. W. Dromerick, "Rehabilitation After Stroke: Current State of the Science," *Current Neurology and Neuroscience Reports*, vol. 10, no. 3, pp. 158–166, Mar. 2010.

[2] N. Hogan, H. I. Krebs, B. Rohrer *et al.*, "Motions or muscles? Some behavioral factors underlying robotic assistance of motor recovery," *The Journal of Rehabilitation Research and Development*, vol. 43, no. 5, p. 605, 2006.

[3] J. F. Schenck, "The role of magnetic susceptibility in magnetic resonance imaging: MRI magnetic compatibility of the first and second kinds." *Medical Physics*, vol. 23, no. 6, pp. 815–850, 1996.

[4] S. Menon, G. Brantner, C. Aholt, K. Kay, and O. Khatib, "Haptic fMRI : Combining Functional Neuroimaging with Haptics for Studying the Brain's Motor Control Representation," in *35th IEEE EMBS Conference*, Jul. 2013, pp. 1–6.

[5] R. Gassert, L. Dovat, O. Lambercy, *et al.*, "A 2-DOF fMRI Compatible Haptic Interface to Investigate the Neural Control of Arm Movements," in *IEEE International Conference on Robotics and Automation*, Apr. 2006, pp. 3825–3831.

[6] N. Yu, C. Hollnagel, A. Blickenstorfer, S. S. Kollias, and R. Riener, "Comparison of MRI-Compatible Mechatronic Systems With Hydrodynamic and Pneumatic Actuation," *IEEE/ASME Transactions on Mechatronics*, vol. 13, no. 3, pp. 268–277, May 2008.

[7] A. Khanicheh, D. Mintzopoulos, B. Weinberg, A. A. Tzika, and C. Mavroidis, "MR-CHIROD v.2: Magnetic Resonance Compatible Smart Hand Rehabilitation Device for Brain Imaging," *IEEE Transactions on Neural Systems and Rehabilitation Engineering*, vol. 16, no. 1, pp. 91–98, 2008.

[8] H. Elhawary, Z. T. H. Tse, A. Hamed, *et al.*, "The case for MR-compatible robotics: a review of the state of the art." *International Journal of Medical Robotics*, vol. 4, no. 2, pp. 105–113, May 2008.

[9] N. Hogan and S. P. Buerger, "Interaction Control." CRC Handbook on Robotics and Automation, Ch. 19, Aug. 2005, pp. 1–24.

[10] J. Izawa, T. Shimizu, H. Gomi, and S. T. K. Ito, "MR Compatible Manipulandum with Ultrasonic Motor for fMRI studies," in *Proceedings of the 2006 IEEE International Conference on Robotics and Automation*, Apr. 2006, pp. 1–5.

[11] M. Flueckiger, M. Bullo, D. Chapuis, R. Gassert, and Y. Perriard, "fMRI compatible haptic interface actuated with traveling wave ultrasonic motor," in *Industry Applications Conference, 2005.*, 2005, pp. 2075–2082.

[12] J. Diedrichsen, Y. Hashambhoy, T. Rane, and R. Shadmer, "Neural correlates of reach errors," *J Neuroscience*, vol. 25, no. 43, pp. 9919–9931, Sep. 2005.

[13] Sergi, F. Krebs, H. I. Groisser, *et al.*, "Predicting Efficacy of Robot-Aided Rehabilitation in Chronic Stroke Patients Using an MRI-Compatible Robotic Device," *Proceedings of the International IEEE EMBS Conference*, pp. 7470–7473, Jun. 2011.

[14] R. M. Birn, R. W. Cox, and P. A. Bandettini, "Experimental designs and processing strategies for fMRI studies involving overt verbal responses," *NeuroImage*, vol. 23, no. 3, pp. 1046–1058, Nov. 2004.

[15] M. M. Williamson, "Series Elastic Actuators," *PhD thesis, MIT*, pp. 1–83, 1995.

[16] J. Rosen, J. C. Perry, N. Manning, S. Burns, and B. Hannaford, "The human arm kinematics and dynamics during daily activities-toward a 7 DOF upper limb powered exoskeleton," *Advanced Robotics, 2005*, pp. 532–539, 2005.

[17] A. Gupta, M. K. O'Malley, V. Patoglu, and C. Burgar, "Design, Control and Performance of RiceWrist: A Force Feedback Wrist Exoskeleton for Rehabilitation and Training," *The International Journal of Robotics Research*, vol. 27, no. 2, pp. 233–251, Feb. 2008.

[18] H. I. Krebs, B. T. Volpe, D. Williams, J. Celestino, S. K. Charles, D. Lynch, and N. Hogan, "Robot-Aided Neurorehabilitation: A Robot for Wrist Rehabilitation," *IEEE Transactions on Neural Systems and Rehabilitation Engineering*, vol. 15, no. 3, pp. 327–335, Dec. 2007.

[19] F. Sergi, A. Erwin, and M. K. O'Malley, "Interaction control capabilities of an MR-compatible compliant actuator for wrist motor protocols during continuous fMRI," *submitted to the IEEE/ASME TRANSACTIONS ON MECHATRONICS*.

[20] V. Agrawal, W. J. Peine, and B. Yao, "Modeling of transmission characteristics across a cable-conduit system," *Robotics, IEEE Transactions on*, vol. 26, no. 5, pp. 914–924, 2010.

[21] S. Wang, C. Meijneke, and H. van Der Kooij, "Modeling, design, and optimization of Mindwalker series elastic joint." *International Conference on Rehabilitation Robotics* vol. 2013, pp. 1–8, 2013.

[22] V. Agrawal, B. Yao, and W. J. Peine, "Modeling of Viscoelastic Cable-Conduit Actuation for MRI Compatible Systems," *Journal of Dynamic Systems, Measurement, and Control*, vol. 135, no. 5, p. 051004, Sep. 2013.

[23] V. Agrawal, W. J. Peine, B. Yao, and S. Choi, "Control of cable actuated devices using smooth backlash inverse," in *Robotics and Automation (ICRA), 2010 IEEE International Conference on*. IEEE, 2010, pp. 1074–1079.

[24] R. S. Barbosa and J. T. Machado, "Describing function analysis of systems with impacts and backlash," *Nonlinear Dynamics*, vol. 29, no. 1-4, pp. 235–250, 2002.

[25] H. Vallery, J. Veneman, E. van Asseldonk, R. Ekkelenkamp, M. Buss, and H. van Der Kooij, "Compliant actuation of rehabilitation robots," *Robotics & Automation Magazine, IEEE*, vol. 15, no. 3, pp. 60–69, Jan. 2008.